

# Voltage asymmetry in the current-voltage characteristics of granular $\text{YBa}_2\text{Cu}_3\text{O}_{7-\delta}$ at very low magnetic fields

M. T. González, S. R. Currás, J. Maza, and F. Vidal

*LBTS,\* Departamento de Física da Materia Condensada, Universidade de Santiago de Compostela, Santiago de Compostela, E15706, Spain*

(Received 18 February 2000; revised manuscript received 27 November 2000; published 23 May 2001)

We study the current-voltage characteristics (CVC's) in granular  $\text{YBa}_2\text{Cu}_3\text{O}_{7-\delta}$  under applied magnetic fields with an amplitude and a spatial distribution similar to the self-fields generated by the transport currents. By this way, a proper compensating procedure between both fields has allowed us to obtain CVC's at a very low *constant* resultant field. To that end, hollow cylinder-shaped samples were axially threaded by an external wire in a counter-current setup. The measurement procedure lay in applying a variable magnetic field by the external wire compensating the increasing self-field. CVC's in the range 2–20 Oe, even below the sample self-field, were thus obtained, with voltage spanning three orders of magnitude. A relevant result from these measurements is the different voltage values observed for resultant field distributions of the same root-mean-square volume average but opposite azimuthal polarity. This asymmetry may find an explanation in terms of a concentration of the current in between the grains giving an effective magnetic field different from the macroscopic field. An expression for the effective magnetic field that accounts quantitatively for the data is put forward.

DOI: 10.1103/PhysRevB.63.224511

PACS number(s): 74.25.Fy, 74.60.Jg, 74.50.+r, 74.72.Bk

## I. INTRODUCTION

Current-voltage characteristics (CVC's) are a chief signature of the transport properties of superconductors. Their study under applied magnetic fields has both theoretical and practical relevance, and a wealth of results is available on high- $T_c$  superconductors. However, only a few correspond to the very low magnetic-field regime, meant here as that corresponding to magnetic fields of the order of the sample's self-field, i.e., the magnetic field caused by the transport current itself.<sup>1–9</sup> The study of CVC's in such a very low-field regime is particularly meaningful in the presence of weak links, as it is the case of granular bulk samples, and also any practical cuprate superconductor, where the existence of weak links is almost unavoidable. Apart from the interest of these constant-field measurements to characterizing the electrical transport properties of granular high- $T_c$  superconductors, new CVC results in the magnetic-field range of interplay of the applied field with the self-field may also provide useful information on general aspects of the weak links behavior in these materials. On recognizing the overall behavior of a bulk high- $T_c$  superconductors as a collection of grain boundary junctions, one should expect that interplay to be as meaningful as it is for single Josephson junctions.<sup>10</sup>

In previous works, the CVC's in these materials have been measured at a constant applied magnetic field, and hence the increasingly important self-field contribution along a CVC (just due to the increasing transport current) does not guarantee the constancy of the total magnetic field. Consequently, current effects and magnetic field effects are intermixed in those measurements. The magnetic field effects in the very low-field regime can only be separated from current effects if a proper applied field allows for a compensation of the self-field.

In this paper, we have implemented an experimental setup that allows a proper compensation of the self-field so that the

resultant field can be clamped along a CVC. We present a systematic study of the CVC's of a batch of granular  $\text{YBa}_2\text{Cu}_3\text{O}_{7-\delta}$  samples at the very low magnetic-field range 2–20 Oe in conditions of constant total (self+applied) magnetic field. The results will be compared with the extended Ambegaokar-Halperin model. Ideas in the framework of local field models are put forward to bring theory to accord with measurements.

## II. EXPERIMENTAL DETAILS

### A. Experimental setup and measurement protocol

The study of CVC's under very low magnetic field was carried out under cylindrical symmetry for both the sample geometry and the applied field. Cylinder-shaped samples of outer radius  $r_e = 2.5$  mm were used, details of whose synthesis will be given later. The samples were axially drilled so as to produce a longitudinal hole of radius  $r_i = 0.75$  mm, along which a copper wire was threaded. This copper wire was used to apply an external magnetic field. With this arrangement (see Fig. 1) both the sample self-field and the external field share the same cylindrical symmetry and, as a result, control of the total magnetic field is made easier.

As for the measurement systematics, two independent dc current sources were used to inject the sample current and the external current, as schematized in Fig. 1. The sources were operated discontinuously, in a pulselike manner, to minimize spurious heating at the current pads. Two stable in-series resistors were immersed together with the sample into the nitrogen bath to measure the current in both the sample and the axial copper wire. In that way, around a hundred points per CVC curve were taken.

The experimental setup just described, corresponds to the so-called “counter-current arrangement,” which has been used early by Zhukov and coworkers<sup>11</sup> and then by other authors<sup>12</sup> for the study of critical currents and critical state

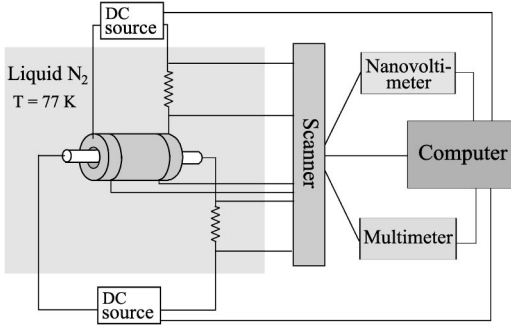


FIG. 1. Counter-current setup implemented in this work to allow for a proper compensation of the sample self-field. A controllable external current flows through hollow cylinder-shaped samples to produce a magnetic field with the same symmetry. In this way, the current-voltage characteristics at constant resultant magnetic field in the range 2–20 Oe were measured for a batch of  $\text{YBa}_2\text{Cu}_3\text{O}_{7-\delta}$  nitrogen-cooled samples.

models. However, in our experiments, not only the voltage threshold but also the whole CVC has been measured at total (self-field+applied field) magnetic field constant (see Fig. 3). We describe thus how the CVC's were obtained.

The voltage  $V$  at the sample ends will depend on the current flowing through the sample  $I$ , and some average of the magnetic field over the sample's volume, which is associated with both the current through the sample,  $I$ , and the current through the copper wire  $I_w$ . The root-mean-square (rms) average of the magnetic field is the direct candidate both for its analytical simplicity and its relevant meaning of magnetic energy. The effects of choosing other possibilities will later be considered. We want to advance that out-detailed analysis later in the paper does not rely on any magnetic field criterion.

In our particular case, the rms averaged field reads

$$H_{\text{rms}} = \left[ \frac{1}{S} \int_S (H_{\text{app}} + H_{\text{self}})^2 dS \right]^{1/2}, \quad (1)$$

where  $H_{\text{app}}$  is the applied field associated with  $I_w$ , and  $H_{\text{self}}$  is the field whose source is the transport current,  $I$ .

Our mean restrain, namely constant-field during all the CVC's, requires the application of the proper copper wire current,  $I_w$  for each value of  $I$ , so that  $H_{\text{rms}}$  remains constant. As a first approximation, the contribution of the self-field,  $H_{\text{self}}$ , to  $H_{\text{rms}}$  was calculated under a constant current density. From elementary electromagnetics one gets:

$$H_{\text{app}}(r) + H_{\text{self}}(r) = \frac{2\mu_0}{r} \left( I_w + \frac{r^2 - r_i^2}{r_e^2 - r_i^2} I \right), \quad (2)$$

for the magnetic field at radial coordinate  $r$ . Whence, by a trivial integration:

$$H_{\text{rms}} = [AI_w^2 + BI^2 + CI_w I]^{1/2}, \quad (3)$$

with  $A$ ,  $B$ , and  $C$  being geometrical factors depending on  $r_e$  and  $r_i$ .

For the explored magnetic fields  $2 < H_{\text{rms}} < 20$  Oe and current intensities  $0 < I < 10$  A, the current in the copper

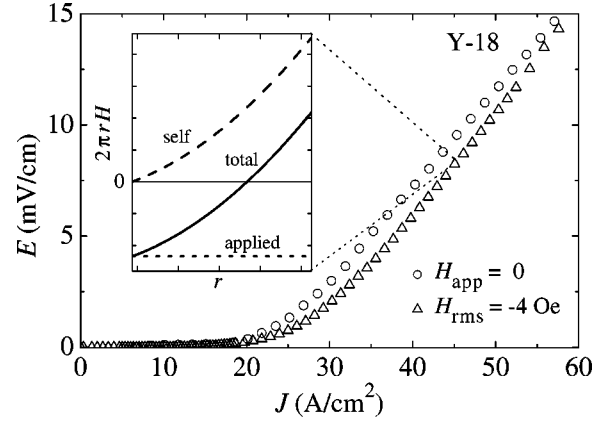


FIG. 2. Shift on a typical current voltage curve caused by the application of a counter current. Note that the plotted self-field makes up the total field for the circle point at the same sample current ( $H_{\text{app}} = 0$  curve). The inset is a map of the fields corresponding to the triangle point indicated.

wire spans the range  $-20 < I_w < 20$  A. Notice the double-solution feature of Eq. (3): at a given sample current, there are two external currents giving the same rms total magnetic field,

$$I_w = -\frac{C}{2A} I \pm \left[ \left( \frac{C^2}{4A^2} - \frac{B}{A} \right) I^2 - \frac{1}{A} H_{\text{rms}}^2 \right]^{1/2}. \quad (4)$$

If we define the sample current as positive, the higher  $I_w$  is positive for most of the solution space. In turn, the solution of lower  $I_w$  (but greater in absolute value) is mostly negative, i.e., it acts as a counter current. As the correlation in sign of  $I$  and  $I_w$  is inherited by their corresponding magnetic fields, we will call *positive-field (negative-field) CVC branch* the current-voltage characteristics obtained when the applied field is such that the resultant field is parallel (antiparallel) to the sample self-field. In that way, though a rms field value is positive defined, we will use signed rms values as a short notation to comprise both CVC branches. Before presenting the systematic measurements performed it can be of help to illustrate how and to what extent the field compensation works. This is done in Fig. 2, showing the partial self-field cancelation at any radial coordinate within the sample. Note that at any sample current the electrical voltage gets lower under the application of the appropriate external field.

## B. Preparation and characterization of the samples

The polycrystalline YBCO samples used in this work were sinterized by the conventional ceramic process. Powder was furnace several times at 950 °C for 12 h after corresponding grinding. Sintering took place in air at 910–930 °C for different time intervals between 1–24 h in order to get samples with different resistivities. The samples were axially drilled into a 1.5 mm dia hole and then oxygenated at 400 °C for 24 h. Electrical contacts were made by silver evaporation to get 1–1.5  $\mu\text{m}$  thick pads, followed by an annealing at 340 °C for 1 h. Then, copper wires were glued

TABLE I. Some characteristic quantities for the four granular  $\text{YBa}_2\text{Cu}_3\text{O}_{7-\delta}$  samples studied in this work as follows: The critical current density at self-field for a threshold criterion of  $1 \mu\text{V}/\text{cm}$ . The transition temperature  $T_{\text{CI}}$ . The transition width  $\Delta T_{\text{CI}}$ . The normal-state resistivity slope with temperature  $\rho'_n$ . The extrapolation of the normal-state resistivity to zero temperature  $\rho_n(0)$ . The paracoherent resistivity  $\rho_p$ , which is obtained from the slope of the current-voltage characteristics. The last column shows the close correlation between the two last quantities.

Sample	$J_C$ ( $\text{A}/\text{cm}^2$ )	$T_{\text{CI}}$ (K)	$\Delta T_{\text{CI}}$ (K)	$\rho'_n$ ( $\mu\Omega \text{ cm}/\text{K}$ )	$\rho_n(0)$ ( $\text{m}\Omega \text{ cm}$ )	$\rho_p$ ( $\text{m}\Omega \text{ cm}$ )	$\rho_n(0)/\rho_p$
Y-18	6.7	91.2	0.5	10.8	1.9	0.35	5.4
Y-1a	11.2	91.3	0.3	4.7	0.78	0.13	6.0
Y-24	16.2	91.0	0.6	8.3	0.61	0.14	4.4
Y-1b	39.7	90.5	0.6	4.1	0.43	0.078	5.5

to the pads using silver paste. Contact resistivities of  $10^{-4}$ – $10^{-5} \Omega \text{ cm}^2$  were so achieved.

Normal-state resistivity measurements were routinely made to record the granularity characteristics of the samples. Table I summarizes the more relevant charge transfer characteristics of the samples used in this work.

### III. CVC MEASUREMENTS. VOLTAGE ASYMMETRY UNDER FIELD REVERSAL

The measured CVC's at various positive and negative total rms averaged magnetic fields for a representative sample are shown in Fig. 3. These curves are to our knowledge the first available CVC's at very low constant magnetic field.

The general trend of the data in Fig. 3 is qualitatively coincident with those obtained at higher fields in granular high- $T_C$  compounds.<sup>5,13,14</sup> In particular, the resistivity is shown to converge to a field- and current-independent value  $\rho_p$  at high current, typical of granular media (see also the insets of Fig. 3).<sup>4,7,13,15</sup> This regime, known as *paracoherent state*, is characterized by the switching of the grain-boundary junction to the normal state while the intragrain material rests superconducting. The values of the paracoherent resistivity,  $\rho_p$ , for the samples in this work are displayed on the sixth column of Table I. In a previous paper, we have put forward a correlation between this paracoherent resistivity and the zero-intercept of the normal-state resistivity,  $\rho_n(0)$ :  $\rho_n(0)/\rho_p = f$ , being  $f$  a structural factor only dependent on the grain morphology.<sup>16</sup> In the present case, last column of Table I shows that the ratio  $\rho_n(0)/\rho_p$  is indeed constant to a very good approximation.

In spite of the expected qualitative similarity of the two sets of CVC's on Fig. 3, there are also quantitative and systematic differences. In particular, it is clearly seen that voltages at the same sample current and total rms averaged magnetic field are lower for the negative-field branch than for the positive-field branch. In a certain abuse of language, we will refer to this situation as *field reversal asymmetry*. In order to avoid misinterpretation, we emphasize that the observed voltage asymmetry has nothing to do with: (i) changing simultaneously the sense of the external and sample's current, in which case voltage should be obviously the same but opposite in sign; and (ii) changing only the sense of the external current, whereby the voltage would evidently change be-

cause of the change in the total field (first reports of this "first-order effect" may be seen in Ref. 11). It is also worth noting here the fact that no hysteretic effect is involved in the voltage asymmetry, because no such effects have been found under careful checking. However, no contradiction exists with available reports on hysteretic behavior of voltage on field cycled from 0 to 800 Oe and back because of the much less magnitude of the maximum field used in our work.<sup>17</sup>

Figure 4 singles out the asymmetric CVC response under

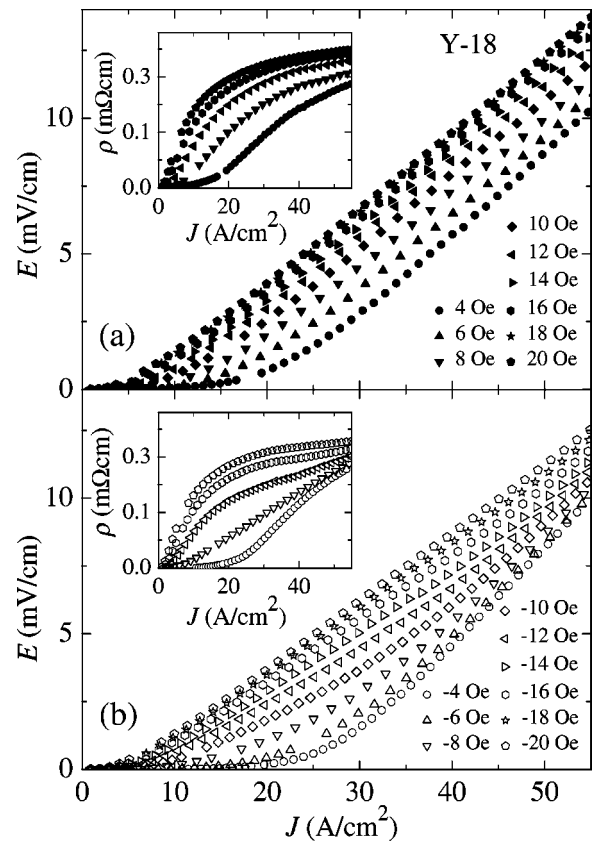


FIG. 3. CVC's for a representative granular  $\text{YBa}_2\text{Cu}_3\text{O}_{7-\delta}$  sample at various very low constant magnetic fields. The curves in (a) and (b) correspond to the positive-field and negative-field branches, respectively. The resistivities  $\rho = E/J$  plotted in the insets show the tendency towards the (Ohmic) paracoherent state at high current.

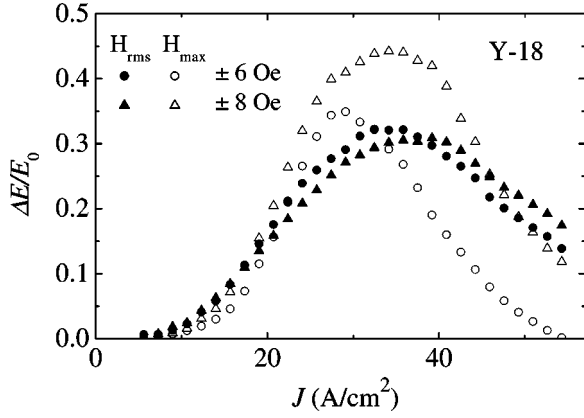


FIG. 4. This figure plots the asymmetry in the CVC's under magnetic-field reversal. In the vertical axis,  $\Delta E$  is the difference in the electric fields of the positive- and negative-field branches for two distinct criteria for characterizing the magnetic field, and  $E_0 = E(J = 40 \text{ A/cm}^2)$ . The solid symbols correspond to the root-mean-square criterion and are obtained from Fig. 3, whereas the open symbols correspond to the maximum field criterion (see text for details). The observed asymmetry is a significant result in that the relative effect  $\Delta E/E_0$  is of the order of some tens per cent.

low magnetic fields by displaying the electric field subtraction  $\Delta E = E_{\text{positive}} - E_{\text{negative}}$  obtained from the data of Fig. 3, as a function of the average current density  $J$  (solid symbols). It can be asked whether the displayed asymmetry is heavily dependent on the magnetic-field criterion used for organizing the points. We have worked out quantitatively the maximum field criterion (maximum of the absolute values of the magnetic field within the sample) and also the absolute-value average. We have seen that the asymmetry keeps nearly at the same value in spite of using such very distinct magnetic-field criteria (the maximum of  $\Delta E/E_0$  of Fig. 4 is always above 20% regardless the criterion used). As an example, the results for the maximum field criterion are shown in open symbols in Fig. 4.

The downturn of voltage asymmetry at high sample's current is mainly due to the drop in the sensitivity of the voltage to magnetic field as the sample reaches the paracoherent state. The challenge is to explain the observed asymmetry at medium self-field values (see Fig. 4). In this range, it is straightforward to see that the self-field is comparable to the external field and, hence, any explanation must include the interplay between both fields. In order to find such explanation, it is useful to bear in mind the two main approximations made so far. First, a constant current density has been needed to ascribe a definite magnetic field value to each experimental point in the CVC's. The inhomogeneity of magnetic field (both self-field and applied field) over the sample requires utilizing some sample-volume average. The use of a field average is our second major approximation.

In the next paragraph, an in-depth analysis on the data that is free from these approximations will be made.

#### IV. DATA ANALYSIS

##### A. Current inhomogeneity at sample scale

A constant current density has been assumed above to compute the sample self-field which, in turn, determines the

copper wire current to be applied to get a preset resultant magnetic field. We know this can not be the case because the sample's cylindrical symmetry is inconsistent with a constant current density: for the electric field to be independent of the radial coordinate  $r$ , it must hold:  $\partial E/\partial j * \partial j/\partial r + \partial E/\partial H * \partial H/\partial r = 0$ , and hence  $\partial j/\partial r \neq 0$  for  $\partial H/\partial r \neq 0$ , as  $\partial E/\partial j$  and  $\partial E/\partial H$  are not vanishing.

The measured CVC's represent an average over the sample volume because neither  $j$  or  $H$  is constant. A proper analysis of the observed CVC's should be built upon the local, i.e., point-to-point, relationship linking electric field  $E$  with  $j$  and  $H$ :  $E(r) = E[j(r), H(r)]$ . The chief point is that this fundamental equation is simply unknown. Consequently, we must use a model that best represents the magnetoresistance of granular superconductors. We think that the Ambegaokar-Halperin (AH) one-junction model,<sup>18</sup> as extended by Tinkham,<sup>19</sup> and then by Soulen and coworkers<sup>13</sup> to include the effects of a magnetic field on a disoriented array of grain boundary junctions, is a best choice to map the whole CVC's. It has been already thoroughly tested against experimental CVC's of different granular high- $T_C$  superconductors.<sup>7,14,21,22</sup> Other models, as the flux-flow model with a distribution of pinning centers,<sup>9</sup> or the gauge glass model,<sup>20</sup> might as well give account of the observed CVC's but only in the more limited range of medium-low voltage (below around 1 mV/cm).

The extended AH model was introduced to account for thermal fluctuations in a Josephson junction. Functionally, it may be expressed as:

$$E_{AH} = \rho_p j_C F(\gamma, j/j_C). \quad (5)$$

Here,  $j_C$  is the critical current density of the junction in the absence of fluctuations. Originally,  $\gamma \propto j_C/T$  was the noise parameter associated to thermal fluctuations. More recently, Soulen and coworkers<sup>13</sup> have reinterpreted  $\gamma$  to include the "magnetic disorder" associated with a magnetic field acting on an array of randomly orientated junctions. Both  $j_C$  and  $\gamma$  being magnetic field dependent, a functional form is needed for them. We have found that the expressions giving the best fitting results to our data are<sup>23-25</sup>

$$j_C = j_{C0} \frac{1}{1 + \left| \frac{H}{H_0} \right|^\beta}, \quad (6a)$$

$$\gamma = \gamma_0 \frac{1}{1 + \left| \frac{H}{H'_0} \right|^{\beta'}}. \quad (6b)$$

Quite similar relationships, which have been previously used by other authors,<sup>13,19,26,27</sup> were also tested with similar but slightly worse results.

Finally, the function  $F$  in Eq. (5) represents a lengthy integral expression whose detailed quotation is not needed for our purposes. Note that there are seven free parameters in all. Equations (5) and (6) define the model we will use to analyze our data. As we intend to make a point-to-point

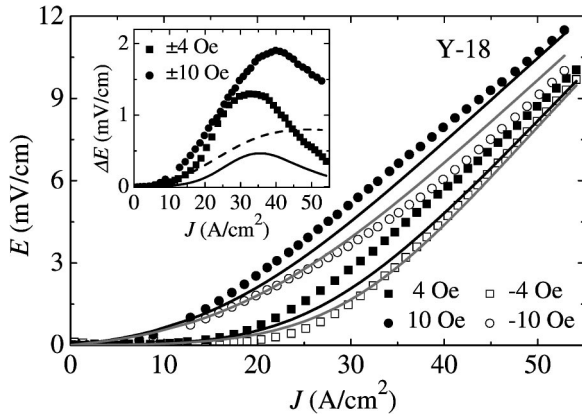


FIG. 5. Least-squares fit of the extended Ambegaokar-Halperin one-junction model to some CVC's corresponding to positive- and negative-field branches. For each point of the CVC's an internal current density and field distributions through the sample must be determined self-consistently with the model (see the text for details). As illustrated in the inset, no satisfying explanation of the voltage asymmetry between both branches is achieved.

analysis, the volume sample was discretized into  $n$  layers. Actually, we take the value of  $n$  as 30, which corresponds to layers of  $60 \mu\text{m}$  approximately. This means that a grain-volume average is involved in the process, consistently with the continuum approach. Other layering spacings were also tried in the analysis to ensure the reliability of the results: from about  $30 \mu\text{m}$ , i.e., not much above the grain size, up to  $400 \mu\text{m}$ , i.e., competing with the sample's wall thickness. The model fitting parameters were found to vary in less than 1%.

In order to obtain the best values for the model parameters, an iterative process was followed through the layers of the sample, with the constrains:

$$E_{AH}[j(r_i), H(r_i)] = E, \quad (7a)$$

$$I_{AH} = \sum j(r_i) 2\pi r_i \delta r_i. \quad (7b)$$

Note that  $H_i$  depends on the actual layer's current density,  $j_i$ , as well as on all the current densities of the previous layers. In this way, the totality of the measured points were analyzed together. In all, fitting the model to the data was an intensive computing-resource consuming task, so that only through parallel supercomputing was the task tractable. Notice that, as a result of this stepping process, each point is now characterized by the directly measurable quantities  $I$ ,  $I_w$ , and  $V$ , rather than by derived quantities under approximations like  $J$  or  $H_{\text{rms}}$ .

The outcome of the fits for a representative sample are depicted in Fig. 5. The global agreement with the extended AH model, whose rms deviation is around 10%, may be thought acceptable. Notwithstanding, Fig. 5 inset shows clearly the theory deficiency in explaining the voltage asymmetry. Not more than around 40% of the average voltage asymmetry finds an explanation in terms of the extended AH model. Other samples showed a slightly better agreement

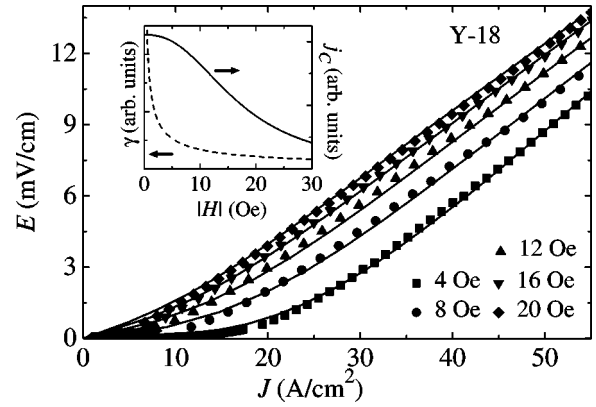


FIG. 6. Fits of the extended Ambegaokar-Halperin one-junction model to some positive-branch CVC's. The displayed excellent quality of the fits to one-branch curves are in contrast to the disagreements in Fig. 5 when both branches are fitted simultaneously. As a by-product, the dependence of the two main parameters of the model on the magnetic field following Eq. (6) are also shown in the inset.

with the model. In sum, only less than half of the average voltage asymmetry under field reversal observed may be accounted for by sample-scale current inhomogeneity.

At this point, it is naturally tempting to argue that we are relying heavily on a particular theoretical model. However, apart from its already invoked adequacy to give account of CVC behavior in many high- $T_C$  materials, the extended AH model fits superbly well our data when only one branch is considered. Figure 6, which shows the fits to only the positive-field branch, is a proof of this fact. The theoretical curves have been obtained by the local fit procedure described above in detail, and are thus the counterparts of those shown in Fig. 5. As we must then recognize, it is the requirement of a simultaneous fit to both CVC branches that causes the relative failure of the AH model to explain the data.

### B. Current inhomogeneity at grain scale and local effective field

The current inhomogeneity at sample scale taken into account so far does not preclude other sources of inhomogeneity at grain scale. Note first that all our measurements have taken place in the paracoherent regime (low current and low magnetic field) for which the grains are in a Meissner state, with neither current nor field inside them. At least two effects can be envisaged that stem from this fact. First, a current inhomogeneity because an applied current will flow in a percolating way only through the "intergranular phase" so that the real current density will be likely higher at the junctions. This would mean enhancing the self field due to a given transport current. Second, on a local scale, screening in superconducting grains results in a local redistribution of the total field, thus increasing the field in between the grains.<sup>28-31</sup>

To take into account the grain-induced current concentration quantitatively is not an obvious task. A clue towards the finding of a proper analytical expression comes out of plotting the threshold critical current  $J_C$  as a function of the rms

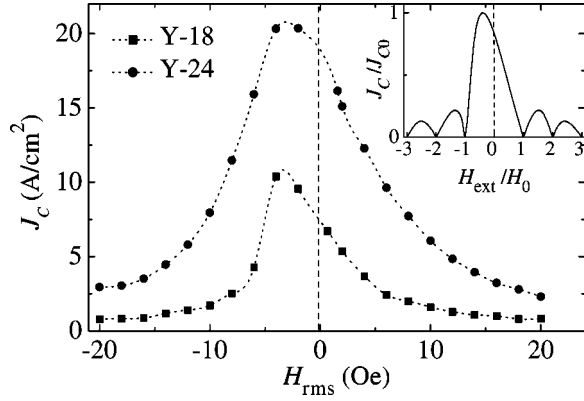


FIG. 7. Threshold critical current ( $1 \mu\text{V}/\text{cm}$  criterion) extracted from both the positive- and negative-field branches of Fig. 3. The dotted lines are only guides for the eye. As clearly seen, the bell-shaped distribution is unexpected in that it is shifted (with respect to the zero rms total magnetic field in the sample) as well as tilted. In order to help analyze the underlying causes, the textbook result for the critical current density of a large Josephson junction under an external magnetic field has also been plotted.

total magnetic field,  $H_{\text{rms}}$  (see Fig. 7).  $J_C$  is the average current density corresponding to a threshold electric field of  $1 \mu\text{V}/\text{cm}$  in the CVC's of Fig. 3. The observed dependence of  $J_C$  on  $H_{\text{rms}}$  in Fig. 7 is very much reminiscent of the dependence of the Josephson current on the external magnetic field  $H_{\text{ext}}$  for a large junction found in textbooks (see, e.g., Ref. 10). This standard result is what has been plotted in the Fig. 7 inset. As it is quite clear, both cases share a similar shift in the maximum of the critical current, as well as a biased shape. In the single junction case, it is the total field, rather than the applied field, the one effective for the large junction, i.e.,

$$H_{\text{ext}} \rightarrow H_{\text{eff}} = H_{\text{ext}} + \alpha J_C, \quad (8)$$

where the term  $\alpha J_C$  measures the junction's self-field contribution at the transition ( $\alpha$  is a geometry dependent parameter). The similarity of behaviors represented in Fig. 7 shows that the rms-averaged magnetic field is not the relevant field for the physics of our granular high- $T_C$  samples, in the same way as the external field is not the relevant field for a large Josephson junction. Obviously, the trivial answer that the field due to the assembly of junctions is not taken into account is unfounded since the rms-averaged total field on the  $x$  axis of Fig. 7 does contain the junctions' self-field. However, because of the qualitative arguments invoked above, the magnetic field actually felt by the grain-boundary junctions is not a macroscopic field  $H$  but an effective field where a modification due to the grain-scale inhomogeneity is to be added. Then, we would be lead to write in our case:

$$H \rightarrow H_{\text{eff}} = H + \alpha j, \quad (9)$$

where  $\alpha$ , probably related with the grain size of the sample, is a priori unknown and will be sample dependent. Notice that the correction in Eq. (9) works in the good sense to explain our results: the total field will be increased by this self-field enhancement in the positive branch, whereas it will

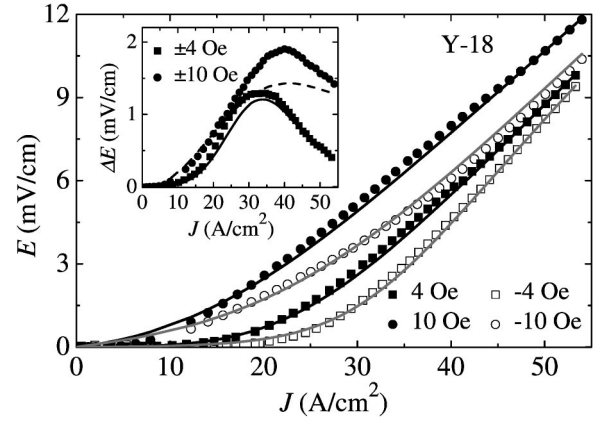


FIG. 8. Comparison of the CVC measurements with the theoretical model made up by the extended Ambegaokar-Halperin model plus self-field enhancement through local effects (see the text for details). The inset shows up the difference in voltage between the positive and negative branches. The excellent fit quality in this figure is to be confronted with that in Fig. 5 where no local effects were included.

be decreased in the negative branch where the total field is antiparallel to the self-field. Thus, voltage will be lower in the positive branch and higher in the negative branch, as observed.

The practical use of Eq. (9) is as simple as writing  $H + \alpha j$  in place of  $H$  in Eqs. (6) and (7) and then remarking the fitting procedure already described. The outcome of the data analysis on the two CVC branches is shown in Fig. 8. As it is observed, the agreement of the model to the data is so much improved as compared with the previous fit in Fig. 5 that a meaningful merit is to be ascribed to the effective field approach. The resultant parameters' values with the so modified model are displayed in Table II. It can be shown that the parameter  $\beta'$  is close to 1 for all samples, which reduces the functional form of  $\gamma$  in Eq. (6b) to the Anderson-Kim expression.<sup>32</sup> On the other hand,  $\beta$  is quite variable from one sample to another and always bigger than 2, a value which has been often reported.<sup>23,24</sup>

The numerical values of  $\alpha$  in Table II show that the correction term is quite relevant because it can amount up to 80% of the average self-field for some of the samples. The

TABLE II. Main data-analysis parameters of the four  $Y$ -based samples studied in this work. The first six columns are quantities associated with the extended AH model. The best fit paracoherent resistivity values are not shown because they are virtually coincident with the CVC's slopes displayed in the sixth column of Table I. The last column displays the values of the self-field enhancement parameter.

Sample	$J_{C0}$ ( $\text{A}/\text{cm}^2$ )	$H_0$ (Oe)	$\beta$	$\gamma_0$	$H'_0$ (Oe)	$\beta'$	$\alpha$ (mm)
Y-18	43.0	20.4	2.7	19.9	2.6	1.2	0.25
Y-1a	49.1	17.0	2.8	27.3	1.2	0.88	0.14
Y-24	55.7	19.6	3.4	26.2	2.9	1.3	0.43
Y-1b	74.7	21.8	6.4	149	1.5	1.4	0.26

fact that  $\alpha$  has length units suggests that it is measuring the length scale which the magnetic local effects are confined into. It can be speculated that  $\alpha$  sets the lower spatial limit for the applicability of continuum media approaches to granular samples. Stated otherwise,  $\alpha$  sets the length scale of the inhomogeneity induced by the grainy structure of granular high- $T_C$  superconductors. In view of the positive sign of  $\alpha$  for all the samples in Table II, we could coin the new contribution in Eq. (9) as a *self-field enhancement by grain-induced current concentration*.

Note finally that this quantitative analysis is just a rough approach to deal with the grain induced current concentration and local-field redistribution, as mentioned at the beginning of the section. These effects occur at a grain scale and, consequently, any description based on macroscopic, i.e., grain-averaged, quantities should be looked on as uncomplete. These limitations can be traced back, for instance, to Eq. (9) where it would seem that Maxwell laws do not apply because the effective macroscopic field is not directly connected with  $j$  through them. Rather, it is our best description replacing an exact but intractable grain scale treatment. In fact, alternative explanations are not free from difficulties. For instance, one could argue that the grain-induced corrections should be simply expressed in terms of current, i.e.,  $j \rightarrow j_{eff} = (1 + \alpha')j$ . Though, as we have verified, similar quantitative results as with Eq. (9) are obtained, an effective cross section of the sample must be included to consistently normalize to the observed current intensity.

A fairly complete picture of the asymmetry effects should then be based on a local scale approach (likely by simulations) but this is far beyond the scope of this paper.

## V. CONCLUSIONS

The current-voltage characteristics (CVC's) of bulk granular  $\text{YBa}_2\text{Cu}_3\text{O}_{7-\delta}$  samples have been measured at very low magnetic field (between 2 and 20 Oe). A distinctive feature regarding previous similar works is the application of an external field to compensate for the increasing self-field along a CVC. This partial compensation occurs because in our experimental arrangement the spatial distributions of the

self-field and the external field are alike. For any current through the sample, our experimental setup allowed to apply two fields leading to the same average resultant (external + self) field but with opposite azimuthal polarity. We have called branches the CVC's obtained at each of the two rms-equivalent fields. Our main finding is the observation of a dissimilar behavior of voltage for the two branches at any current.

Since different current distributions within the sample can eventually be associated with the same rms-average magnetic field but different voltages, it has been necessary to study the spatial distribution of current density. As the current density map can only be made by a model comparison, the extended Ambegaokar-Halperin model has been used for that purpose. The outcome of this analysis is twofold: for either CVC branch a current density distribution can be found that accounts quite well for its observed behavior. No current distributions uniform at grain-size scale able to explain both CVC branches simultaneously can be found.

Our results may find a quantitative explanation on assuming a further inhomogeneity at grain-size scale, namely, a current concentration at the grain junctions induced by the Meissner state of the intragrain material. In more precise terms, the effective self-field at the junctions is not just the macroscopic field due to the transport current,  $H_{self}$ , but the combination  $H_{self} + \alpha j$ , where  $j$  is the current density, and  $\alpha$  is a sample dependent parameter which is probably related to the length scale of the applicability of continuum approaches to granular media. Further work should be carried out to deepen into the physics behind the self-field enhancement effect as well as to find a correlation of the governing parameter  $\alpha$  with other material parameter like grain size. It would be also enlightening to extend the measurements here to other less grainy materials such as films or melt-processed bulk high- $T_c$  superconductors.

## ACKNOWLEDGMENTS

This work was financed by the Xunta de Galicia (XUGA20604B98), CICYT (MAT98-0371), and Unión Fenosa (Contract No. 0666-98) Spain.

\*LBTS (Laboratorio de Baixas Temperaturas e Supercondutividade) is associated with the Consejo Superior de Investigaciones Científicas (Spain).

<sup>1</sup>R.L. Peterson and J.W. Ekin, *Physica C* **157**, 325 (1989).

<sup>2</sup>A.D. Caplin, S.S. Bungre, S.M. Cassidy, J.R. Lavery, and Z.X. Shen, *Physica A* **168**, 268 (1990).

<sup>3</sup>E. Babić, M. Prester, N. Biškup, Ž. Marohnić, and S.A. Siddiqi, *Phys. Rev. B* **41**, 6278 (1990).

<sup>4</sup>W.M. Tiernan and R.B. Hallock, *Phys. Rev. B* **43**, 10 508 (1991).

<sup>5</sup>H.S. Edelman and D.C. Larbalestier, *J. Appl. Phys.* **74**, 3312 (1993).

<sup>6</sup>S. Schattemburg, H. Kliem, and W. Banhofer, *J. Appl. Phys.* **76**, 1116 (1994).

<sup>7</sup>D.A. Komarkov, A.A. Zhukov, and J. Mirkovic, *Solid State Commun.* **89**, 751 (1994).

<sup>8</sup>J. Everett, M. Dhallé, M.D. Johnston, A.D. Caplin, J.C. Moore, S.

Fox, D. Hyland, and C.R.M. Grovenor, *Supercond. Sci. Technol.* **9**, 1077 (1996).

<sup>9</sup>A. Kiliç, K. Kiliç, S. Senoussi, and K. Demir, *Physica C* **294**, 203 (1998).

<sup>10</sup>A. Barone and G. Paternó, *Physics and Applications of the Josephson Effect* (John Wiley and Sons, New York, 1982), Chaps. 4 and 5.

<sup>11</sup>A.A. Zhukov, D.A. Komarkov, V.V. Moshchalkov, V.A. Rybachuk, V.V. Snegirev, and V.P. Shabatin, in *Beijing International Conference on High Temperature Superconductivity, 1989*, edited by Z.X. Zhao, G.J. Cui, and R.S. Han (World Scientific, Singapore, 1990), p. 306.

<sup>12</sup>N.McN. Alford, T.W. Button, D.H. Jones, J.D. Birchall, C.E. Gough, and S.J. Penn, *Cryogenics* **29**, 434 (1990); E.P. Roth, T.C. Bickel, T.J. Gardner, and E.L. Venturini, *ibid.* **32**, 640 (1992).

- <sup>13</sup>R.J. Soulen, Jr., T.L. Francavilla, W.W. Fuller-Mora, M.M. Miller, C.H. Joshi, W.L. Carter, A.J. Rodenbush, M.D. Manlief, and D. Aized, *Phys. Rev. B* **50**, 478 (1994).
- <sup>14</sup>D.H. Liebenberg, R.J. Soulen, Jr., T.L. Francavilla, W.W. Fuller-Mora, P.C. McIntyre, and M.J. Cima, *Phys. Rev. B* **51**, 11 838 (1995).
- <sup>15</sup>M. Giura, S. Sarti, E. Silva, R. Fastampa, F. Murtas, R. Marcon, H. Adrian, and P. Wagner, *Phys. Rev. B* **50**, 12 920 (1994).
- <sup>16</sup>A. Díaz, J. Maza, and F. Vidal, *Phys. Rev. B* **55**, 1209 (1997).
- <sup>17</sup>I. Puica, I. Pop, I. Sirtbat, G. Ciobarm, P. Mazzeti, and I.M. Popescu, *Supercond. Sci. Technol.* **9**, 517 (1996).
- <sup>18</sup>V. Ambegaokar and B.I. Halperin, *Phys. Rev. Lett.* **22**, 1364 (1969).
- <sup>19</sup>M. Tinkam, *Phys. Rev. Lett.* **61**, 1958 (1988).
- <sup>20</sup>R.J. Joshi, R.B. Hallock, and J.A. Taylor, *Phys. Rev. B* **55**, 9107 (1997).
- <sup>21</sup>A.C. Wright, K. Zhang, and A. Erbil, *Phys. Rev. B* **44**, 863 (1991).
- <sup>22</sup>J.D. Hettinger, K.E. Gray, D.J. Miller, D.H. Kim, D.G. Steel, B.R. Washburn, J. Sharping, C. Moreau, M. Eddy, M.E. Tkaczyk, J. DeLuca, J.H. Kang, and J. Talvacchio, *Physica C* **273**, 275 (1997).
- <sup>23</sup>A.A. Zhukov, V.V. Moshchalkov, D.A. Komarkov, V.P. Shabatin, A.A. Bush, S.N. Gordeev, and D.V. Shelomov, *Jpn. J. Appl. Phys., Part 2* **29**, L760 (1990).
- <sup>24</sup>S.L. Ginzburg, V.P. Khavronin, G.Yu. Logvinova, I.D. Luzyanin, J. Herrmann, B. Lippold, H. Börner, and H. Schmiedel, *Physica C* **174**, 109 (1991).
- <sup>25</sup>K.-H. Müller, D.N. Matthews, and R. Driver, *Physica C* **191**, 339 (1992).
- <sup>26</sup>C. Gaffney, H. Petersen, and R. Bednar, *Phys. Rev. B* **48**, 3388 (1993).
- <sup>27</sup>M. Xu, D. Shi, and R.F. Fox, *Phys. Rev. B* **42**, 10 773 (1990).
- <sup>28</sup>S.E. Male, J. Chilton, A.D. Caplin, C.N. Guy, and S.B. Newcomb, *Supercond. Sci. Technol.* **2**, 9 (1989).
- <sup>29</sup>S. Senoussi, C. Aguilon, and S. Hadjoudj, *Physica C* **175**, 215 (1991).
- <sup>30</sup>F. Stucki, J. Rhyner, and G. Blatter, *Physica C* **181**, 385 (1991).
- <sup>31</sup>M. Basso, L. Lambardi, S. Marini, M. Marinelli, and A. Morpurgo, *Appl. Supercond.* **2**, 71 (1994).
- <sup>32</sup>Y.B. Kim, C.F. Hempstead, and A.R. Strnad, *Phys. Rev. Lett.* **9**, 306 (1962); P.W. Anderson, *ibid.* **9**, 309 (1962).